CJC Chinese Journal of Chemistry 中国化学 - An International Journal

For submission: https://wiley.atyponrex.com/journal/CJOC
For published articles: https://onlinelibrary.wiley.com/journal/16147065

Concise Report

Cite this paper: *Chin. J. Chem.* **2025**, *43*, 1190—1198. **DOI: 10.1002/cjoc.202401192**

Probing the Structure and Dynamics of the $[NH_4]M(HCO_2)_3$ Ferroelectric Phases: Dielectric Relaxation through Orientational Disorder†

Thomas J. Hitchings,[a] Helen M. Wickins,[b] Lydia G. Burley,[a] Silvia C. Capelli,[c] Franz Demmel,[c] Anthony E. Phillips,[d] Paul Hodgkinson,[b] and Paul J. Saines*[,a]

[a] *School of Chemistry and Forensic Science, Ingram Building, University of Kent, Canterbury, Kent, CT2 7NH, United Kingdom*
[b] *Department of Chemistry, Durham University, DH1 3LE, Durham, United Kingdom*
[c] *ISIS Neutron and Muon Facility, Rutherford Appleton Laboratory, Didcot, OX11 0QX, United Kingdom*
[d] *School of Physical and Chemical Sciences, Queen Mary University of London, London, E1 4NS, United Kingdom*

Keywords

Relaxor ferroelectric | Neutron diffraction | NMR spectroscopy | Quasielastic neutron scattering | Density functional theory | Metal-organic frameworks | Transition metals | Solid state structures

Comprehensive Summary

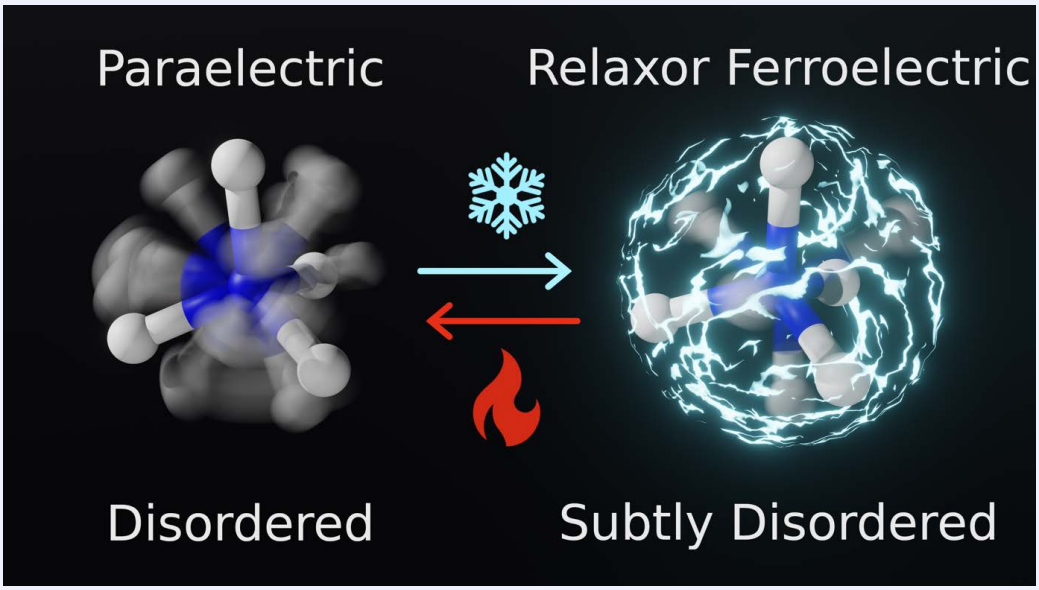

Neutron diffraction studies of the low-temperature relaxor ferroelectric phases of $[NH_4]M(HCO_2)_3$, where M = Mn^{2+} and Zn^{2+}, show that a third of the NH_4^+ cations remain subtly structurally disordered to low temperature. All NH_4^+ cations within the channels are well separated from each other, with significant hydrogen bonds only with the anionic $M(HCO_2)_3$ framework. Complementary studies of the dynamics using ^2H solid state NMR and quasielastic neutron scattering indicate significant rotational motion in both paraelectric and ferroelectric phases, which evolves gradually with increasing temperature with no abrupt change at the phase transition. Nudged elastic band calculations suggest that the activation barrier for flipping between "up" and "down" orientations of the NH_4^+ cations is low in the ferroelectric phase, with the NH_4^+ cations primarily interacting with the framework rather than neighbouring NH_4^+ cations. It is likely this motion that is responsible for scrambling the NH_4^+ cation orientation locally in the ferroelectric phase. We propose that this disorder, with the same basic motion active above and below the phase transition, induces the significant dielectric relaxation in these materials. This suggests that *orientational* disorder may be an effective substitution for *compositional* disorder commonly associated with relaxor ferroelectrics in molecular materials.

*E-mail: P.Saines@kent.ac.uk
† Dedicated to the Special Issue of Emerging Investigators in 2024.

Background and Originality Content

Ferroelectric materials exhibit a spontaneous and switchable polarisation arising from the alignment of electric dipoles with an applied electric field. In most ferroelectrics, the atomic mechanism involves dipoles that are correlated below a symmetry-breaking phase transition: this includes both the displacive transitions common amongst ceramics, such as the widely industrially used $BaTiO_3$,[1-2] and order-disorder transitions in the hydrogen-bonded ferroelectrics Rochelle's salt and K_2HPO_4, which are built from molecular units.[3-4] These phase transitions are associated with a sharp discontinuity in the dielectric permittivity as a function of temperature. On the other hand, *relaxor* ferroelectrics have broad peaks in their temperature dielectric spectra, with the peak temperature depending significantly on frequency; most such materials are ceramic or organic polymer based systems that show no bulk symmetry change in the temperature range in which their dielectric constants peak.[5-8] Relaxor ferroelectrics are desirable materials for harvesting waste mechanical energy, high power energy storage in capacitors and ultrasound sensing applications, due to their large dielectric constants and piezoelectric responses. In addition, the broad temperature range over which they exhibit their high dielectric responses offers a wider operational window for functional devices.[9] Common drawbacks of such materials are that they are usually Pb based (and many lead-free alternatives still contain heavy metals) and most suffer electromechanically induced strain.[7,9]

In established families of relaxor ferroelectrics, the relaxor behaviour is almost ubiquitously associated with compositional inhomogeneity. For example, ceramic oxide relaxors are usually perovskites with a complex mixture of positionally disordered cations on their A and B sites; while in wholly organic polymer relaxors, inhomogeneity is achieved through a distribution of different functional groups.[6,10-11] This gives rise to a domain structure associated with the temperature and frequency dependence of the dielectric properties. There has been much recent interest in hybrid ferroelectrics, comprised of both inorganic and organic components. Several such materials show dielectric spectra characteristic of relaxor behaviour.[12-17] Such hybrid ferroelectric materials exhibit high mechanical flexibility and facile synthesis along with several shown to exhibit higher dielectric and piezoelectric constants than polymer relaxors, thus making these promising materials for energy harvesting and storage, including for wearable devices. Unlike known relaxors, however, these inorganic-organic hybrid ferroelectric materials are not doped and show no compositional disorder (similar behaviour has also been reported in a homogeneous molecular organic solid[18]). The origin of the relaxor-like properties in these materials therefore remains unclear.[19-22]

We have recently highlighted that the relaxor-like dielectric properties of $[NH_3NH_2]Mg(HCO_2)_3$ are likely caused by the polar phase featuring a mixture of $NH_3NH_2^+$ cations that are perpendicular and parallel to the channel.[23] The populations appear to interchange in the polar phase, with this orientational disorder giving rise to fluctuating regions of polar $NH_3NH_2^+$ cations aligned along the channels in a matrix of non-polar $NH_3NH_2^+$ cations perpendicular to the channels. This study utilised a mixture of neutron single crystal diffraction, ^2H NMR and quasielastic neutron scattering (QENS), which have particular sensitivity to the cation behaviour across a range of timescales through their sensitivity to hydrogen. The $[NH_4]M(HCO_2)_3$ (M = Mg^{2+}, Mn^{2+}, Fe^{2+}, Co^{2+}, Ni^{2+} and Zn^{2+}) frameworks, which have very similar chiral hexagonal framework structures to $[NH_3NH_2]Mg(HCO_2)_3$, have been reported by Xu *et al*.[12,14] to be relaxor ferroelectrics. The dielectric spectra of the $[NH_4]M(HCO_2)_3$ compounds show relatively broad peaks with frequency dependence indicative of dielectric relaxation; the change in the temperature at which the dielectric response peaks with the electrical field frequency is less in the $[NH_4]M(HCO_2)_3$ series than in $[NH_3NH_2]Mg(HCO_2)_3$.[12,14,24]

The $[NH_4]M(HCO_2)_3$ series adopt a helical anionic $M(HCO_2)_3$ framework, which has a $4^9{\cdot}6^6$ network topology, with hexagonal channels occupied by the NH_4^+ cations.[12,14,24] In the high temperature phase, the NH_4^+ cations are disordered between orientations pointing "up" and "down" the *c*-axis, with the structure having $P6_322$ hexagonal symmetry (see Figure S1).[25] Most of these chiral hexagonal materials show a conventional paraelectric to ferroelectric transition at low temperature associated with the dielectric maxima. This leads to a polar hexagonal $P6_3$ space group at low temperatures with the dielectric maxima being associated with this transition.[25] This is reported to be due to ordering of the cations, changing the single disordered NH_4^+ environment in the paraelectric phase to three crystallographically distinct NH_4^+ environments in the low temperature ferroelectric phase.[12,14,24] Transition temperatures decrease as the metal cation across the series gets smaller;[12,14,26] the phase transition to the polar phase is supressed for the smallest cation Ni^{2+}.[25] Electron paramagnetic resonance measurements on Mn^{2+}-doped $[NH_4]Zn(HCO_2)_3$ indicate the ferroelectric transition is continuous, belonging to a 2D universality class.[27] Further details of this structural phase transition are discussed in the electronic supporting information (ESI).

Like the $[NH_3NH_2]M(HCO_2)_3$ series, the $[NH_4]M(HCO_2)_3$ systems lack cation doping and have an explicit symmetry change at the temperature associated with their dielectric anomaly, which are not features usually associated with relaxors.[9] Understanding the origins of their relaxor-like behaviour requires probing the structures and dynamics of the material beyond what can be gained from initial X-ray crystal structure determination. While initial neutron powder diffraction studies were able to resolve the fine details of the structure of the paraelectric phase, this was inadequate for the more complex polar structure.[25] Similarly, studies of the dynamics of these materials are very limited. Herein, we have employed a similar multi-technique methodology to that we applied to $[NH_3NH_2]Mg(HCO_2)_3$ to gain an understanding of the likely origins of the dielectric relaxation in $[NH_4]M(HCO_2)_3$ with the addition of computational modelling to aid interpretation. Given indications that the size of the B-site cation has a significant effect on the ferroelectric transition, we have focused on the Mn^{2+} and Zn^{2+} members of the series, which have the smallest and largest cation known to undergo the ferroelectric-paraelectric phase transition.

Results and Discussion

Crystal structure

Since the structure of the paraelectric phase has been previously established by powder neutron diffraction,[25] the single crystal neutron diffraction studies presented here focus on the low temperature structure, in which the NH_4^+ cations are ordered. The symmetry of the M = Mn^{2+} and Zn^{2+} phases below the transition temperature, 254 K and 192 K, respectively, is confirmed as $P6_3$, with three crystallographically unique cation environments that sit within the hexagonal channels of the $M(HCO_2)_3$ framework.[12] The elusive proton positions of the NH_4^+ cations were previously determined geometrically by X-ray diffraction using laboratory sources, with low certainty in their positions both because X-rays are relatively insensitive to light atoms and because hydrogen's single electron is located in the covalent bond. The positions of the molecular cations in the polar phase determined by neutron single crystal diffraction are shown in Figures 1 and S2, labelled according to the nitrogen environments (see Table S1 for crystallographic details); we note this technique is particularly sensitive to the N position due to the large neutron scattering length of this element. The N1 cations, which occupy the channels at the vertices of the unit cell, are well ordered along the polar *c*-axis, which corresponds with the sixfold screw axis. The two central channels of the cell contain alternating N2 and N3 ammonium environ-

ments centred on a threefold rotation axis. The two resulting chains of ammonium cations are oriented antiparallel to each other along *c*. This confirms the arrangement modelled by the single crystal X-ray diffraction (SCXRD) experiment.[12]

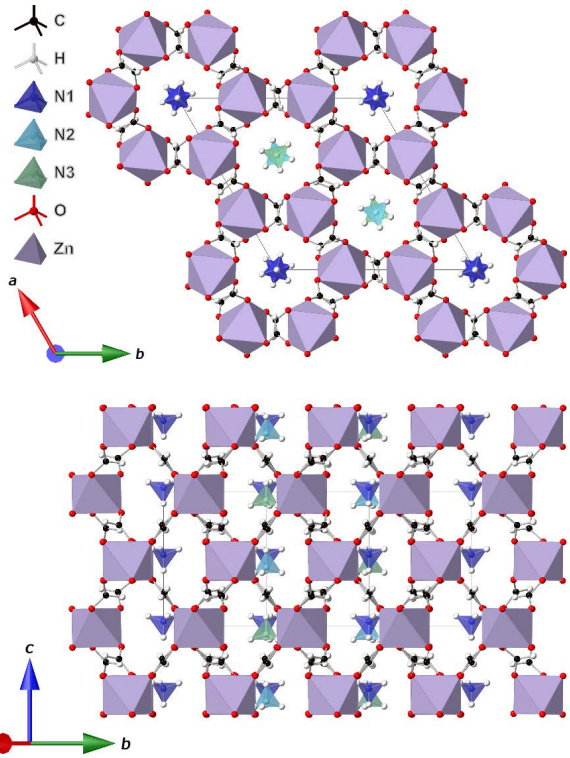

Figure 1 The structural model of the low temperature phase of $[NH_4]Zn(HCO_2)_3$ with the three crystallographically distinct ammonium environments situated in the hexagonal channels of the anionic framework highlighted.

Although the cations appear well ordered in both Zn^{2+} and Mn^{2+} structures, there are weak regions of negative scattering density around the N2 ammonium environment. The position of the negative nucleic scattering for the Mn^{2+} compound suggests rotational disorder of the NH_4^+ protons, primarily affecting the basal sites (see Figure 2 and Figure S3 for the nuclear density difference maps for the final modelled structures). On the other hand, for the Zn^{2+} compound the disorder appears to be associated with tilting of the apical proton off the rotation axis. The N2 cations account for 1/3 of the NH_4^+ groups in the structure and further details of the modelling of this disorder are discussed in the ESI. The N2 environment in the Zn^{2+} analogue has previously been suggested to be likely responsible for the second ^{14}N NMR environment, due to differences in its hydrogen bonding network compared to the other two sites which may be linked to the disorder we observe here.[28]

The hydrogen-bonding interactions in both compounds occur primarily with the framework, suggesting these host-guest interactions are likely responsible for cation ordering (see Tables S2–3 for bond distances and angles). In contrast, the neighbouring cations within each channel are well separated, with the nitrogen atoms in neighbouring cations usually over 4 Å apart. This suggests they may not significantly interact with each other, as is also highlighted from Hirshfeld analysis (see ESI, including Figures S4–5). This lack of interactions between NH_4^+ cations likely plays a role in water molecules being able to insert between ammonium sites in the channels at high humidity.[29] We have previously reported similar shielding of guest disorder by the metal formate framework in the related framework material dimethylammonium manganese(II) formate, which lacks significant hydrogen-bonding or other dipole-dipole interactions between neighbouring molecular cations.[30] In contrast the $[NH_3NH_2]M(HCO_2)_3$ phases have significant hydrogen bonding interactions between the neighbouring molecular cations within their channels in both their antiferroelectric and polar phases.[23,31]

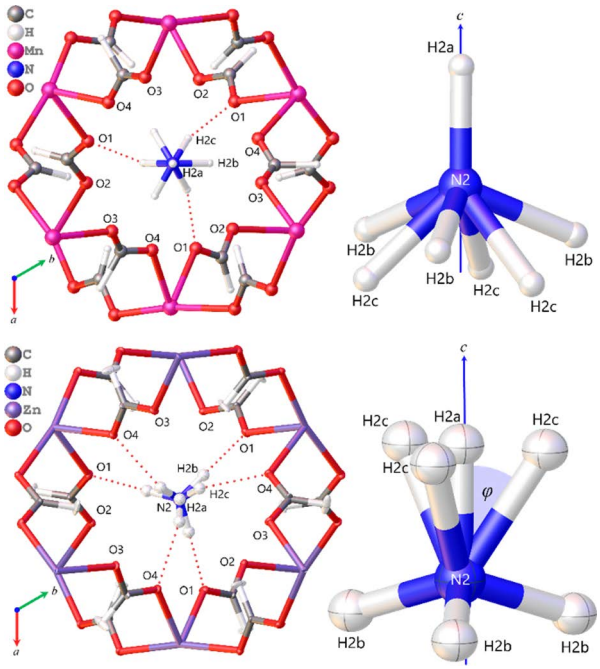

Figure 2 (Top) The Mn^{2+} $P6_3$ phase with hydrogen bonding interactions with the N2 ammonium and framework shown alongside a view of the modellable disorder of the N2 ammonium ion for clarity. (Bottom) The Zn^{2+} $P6_3$ phase with hydrogen bonding interactions with the N2 ammonium and the framework shown alongside the modellable rotational disorder of the N2 ammonium ion shown for clarity. The H2a-N2-H2c angle φ is also highlighted with a value of 34(4)°.

The cell dipole was previously established to arise from an asymmetry of charge distribution in the unit cell caused by the displacement of the NH_4^+ cations in the channels.[12,14] The ammonium displacements calculated from single crystal neutron diffraction, which has greater sensitivity to the N positions, are shown in Table 1. These were determined by measuring displacement relative to the metal cation, which are at equivalent positions in *c* in the paraelectric phases, as previously used by Xu *et al*.[12,14] The overall arrangement has two of the three distinct ammonium cations displaced in one direction. The unit cell polarisation is therefore *ferrielectric*, with oppositely oriented polarisations that do not cancel completely and thus still give an overall cell polarisation. The N atoms displaced in the same direction are N1 and N2 in the Mn^{2+} material and N2 and N3 in the Zn^{2+} material. Interestingly, and consistently with the previous work on this system, this indicates that in the Mn^{2+} material, one of the two distinct NH_4^+ cations sharing a channel moves in the same direction as the cations in the other channel; but in the Zn^{2+} material, the NH_4^+ cations in the same channel all move in the same direction, opposite to those in the other channels. This is consistent with the NH_4^+ cations in each channel having limited interactions with each other, with the positions they adopt at low temperature arising from optimising their interactions with the framework. The absolute values of the displacements of the N1 and N2 nitrogen atoms in the Mn^{2+} material are also more varied from those determined previously by X-ray studies at 110 K, suggesting these may evolve further as the material is cooled to 22 K, as used here.

Solid-state ^2H NMR of $[NH_4]Zn(HCO_2)_3$

The static bandshapes across all temperatures, Figure 3, are very narrow, indicating significant motion, consistent with random

Table 1 Displacement of the nitrogen atoms along the *c*-axis in the $[NH_4]M(HCO_2)_3$ phases obtained from neutron diffraction compared with those determined from the X-ray structure by Xu *et al.*[12]

Atomic site	z coordinate	From SCND at 20 K/ Å	From SCXRD at 110 K[12]/Å
	$[NH_4]Mn(HCO_2)_3$		
Mn	0.432(8)	0	0
N1	0.515(6)	−0.710(8)	−0.406(4)
N2	0.446(8)	−0.120(8)	−0.441(4)
N3	0.372(7)	+0.513(8)	+0.482(4)
Net displacement		−0.317(14)	−0.365(7)
	$[NH_4]Zn(HCO_2)_3$		
Zn	0.4804(5)	0	0
N1	0.5287(6)	+0.3977(6)	+0.397(4)
N2	0.4319(8)	−0.3994(8)	−0.359(7)
N3	0.4338(8)	−0.3837(8)	−0.375(7)
Net displacement		−0.3854(13)	−0.337(11)

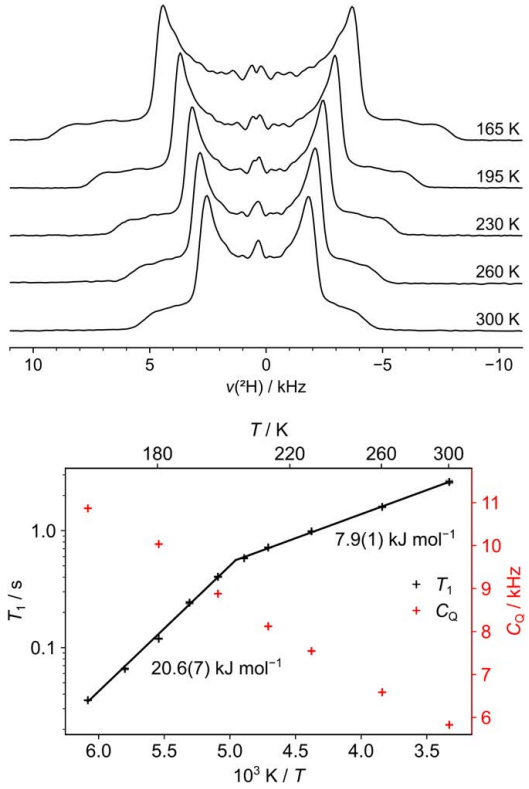

Figure 3 (Top) static SSNMR ^2H spectra and (bottom) T_1 relaxation measurements of $[NH_4]Zn(HCO_2)_3$ at a ^2H NMR frequency of 61.42 MHz. Temperatures are given to the nearest 5 K, reflecting uncertainties in temperature calibration.

re-orientation of all NH_4^+ cations across the full range. The bandshapes become narrower at higher temperatures (*i.e.*, exhibit a smaller averaged C_Q), which implies that motion is slowly approaching quasi-isotropic re-orientation. Interestingly, this increased symmetry is independent of the phase transitions, with a smooth evolution of C_Q observed with increasing temperature. The motion at low temperature is clearly not a single-axis threefold rotation (C_3) jump, which would lead to two distinct spectra: a broad spectrum ~200 kHz wide and a narrow spectrum ~67 = 200/3 kHz wide. Instead, even at low temperature, all the N–H bond vectors must be in exchange at a rate faster than 61 MHz (based on the T_1 data). The residual lineshape after averaging corresponds to an axially symmetric coupling tensor, consistent with the different interactions of the basal versus apical positions with the framework, leading to a non-zero C_Q after motional averaging. Note that NMR cannot determine the exact motional mechanism for the "scrambling" of N–H orientations.

^2H T_1 relaxation measurements showed two regions with a distinct change of gradient either side of ~200 K, corresponding to the crystallographic phase transition at 192 K (see Figure 3). The activation energy for the quasi-isotropic exchange is 20.6 ± 0.7 kJ·mol^{-1} from the low temperature region. The lower activation energy of 7.9 ± 0.1 kJ·mol^{-1} at higher temperature is consistent with motion in the high-temperature paraelectric phase being more energetically favourable.

Quasielastic neutron scattering (QENS)

Evaluation of the mean squared displacement (MSD) parameter with temperature, presented in Figure 4, indicates proton motion becomes sufficiently fast to be detected above 100 K for each system; this is a similar temperature to that at which CH_3 rotations often activate, and is attributed here to the onset of NH_3 rotations.[32] The motion then increases rapidly for each system as it approaches the crystallographic phase transition. This observation is typical, as locally dynamics will speed up as the transition temperature approaches on heating, and the local proton motion will be detected before the bulk phase change.[33] A phase transition will typically involve a sudden increase in the gradient of this curve, as softer modes become activated and the Debye temperature decreases.[34] The MSD increases more gradually at higher temperatures above the phase transition, the decrease in gradient for the Mn^{2+} material occurs immediately following the crystallographically observed phase transition temperature, whilst in the Zn^{2+} material this occurs about 20 K above the phase change (see Figure 4). The higher MSD values in the high temperature phase suggests the motion involves a lower energy barrier in the lower temperature phase, consistent with the significant decrease in activation energy for motion above the phase transition determined by the ^2H SSNMR.

The elastic incoherent structure factor (EISF), which is the proportion of scattering that is elastic as a function of scattering

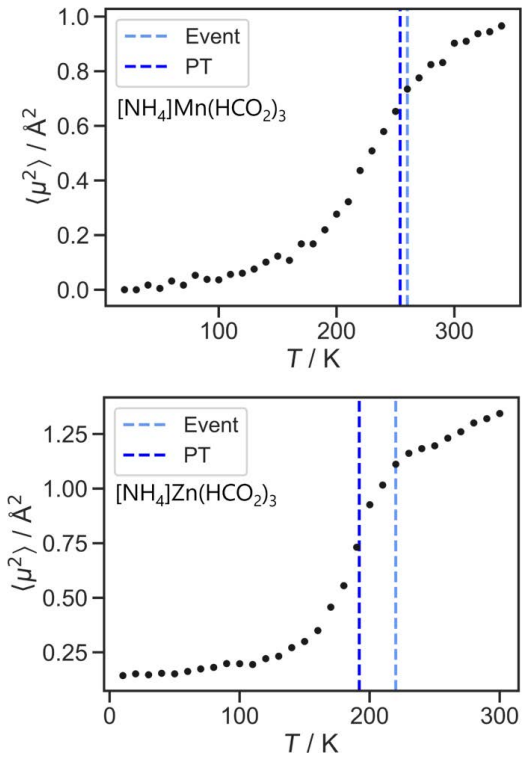

Figure 4 The mean squared displacement of the $[NH_4]M(HCO_2)_3$ frameworks showing the deviation of protons from general positions with increasing temperature for (top) $[NH_4]Mn(HCO_2)_3$ and (bottom) $[NH_4]Zn(HCO_2)_3$. Dark blue dotted lines highlight the crystallographically determined phase transition temperature, with light blue lines highlighting a decrease in the gradient of the plots.

vector *Q* (see Equation S2), can be used to describe the geometry of the rotational diffusion of the NH_4^+ cations about their given centre of mass.[35] As is commonly done to determine the "best" EISF model,[36-39] possible models for the $[NH_4]M(HCO_2)_3$ compounds are presented in Table S4 with representative fits for each model at low temperature and high temperature for M = Zn^{2+} (see Figures S6–8). In each case, the fraction of molecules contributing to the motion, *f*, is refined, along with an empirical correction for multiple scattering effects, *m*, by Equation S3. The data collected with the PG(002) monochromator does not measure to sufficiently high *Q* to allow the models to be distinguished, and the difference between the fits of the different models to the data collected using the PG(004) monochromator is relatively subtle. At low temperatures we employ a model (model **E** in Table S4) that combines threefold rotation around a N–H bond that causes protons to jump between the other three protons sites along with allowing for motion of the formate. The formate contribution is consistent with the significant displacement parameters of the formate proton in the anisotropically refined Zn^{2+} structural model (see Figure 2). At higher temperatures a different model (model **F** in Table S4) is tested which combines a twofold rotation (modelling the "up"/"down" disorder in the high temperature structure) in addition to single-axis threefold rotation. For both models, the radius of the rotational motion of the NH_4^+ cations is fixed from the distances indicated by the neutron crystallography, with the distance for the twofold rotation fixed by the height of the low temperature tetrahedron. The fits for the model to the EISF data at varying temperatures are shown in Figure 5 for both the PG(002) and PG(004) orientations. As only a single Lorentzian peak can be fitted, the QENS models treats the crystallographically distinct NH_4^+ environments as equal across all temperatures. Model **E** fits well to all temperatures and is similar to **F** where this is employed at high temperature. Thus, the EISF data is also consistent with a smooth evolution of the motion across the phase transition rather than a sudden change. While neither model directly matches the quasi-isotropic scrambling indicated by the ^2H NMR the trends we draw from these fits will likely remain correct even if the absolute values determined for *f* and *m* may be somewhat model dependent. An evaluation of *f* between the two compounds shows that the NH_4^+ cations in the Zn^{2+} sample are much more dynamic than in the Mn^{2+} analogue at comparable temperatures. While *f* is usually expected to increase linearly with temperature, this is not observed here (see Table S5 and Figure S9). This is attributed to some fraction of the molecules moving faster than the ~1 ps rate that can be resolved by the dynamic range of the OSIRIS spectrometer. Deviation of the *f*-values from a linear trend with temperature occurs at about the same temperature that the level of the EISF rises, consistent with some fraction of the hydrogen atoms moving faster than the range of the spectrometer. Interestingly, the observed curving of the *f* parameter begins below the crystallographic phase transition temperature, suggesting that the fast motion is already occurring for a fraction of molecules in the ferroelectric phase.

The variation in the Lorentzian width Γ with *Q* is minimal (see Figure S10), suggesting a lack of long-range diffusion, and consistent with localised rotational motion. The increase in Γ with temperature indicates the motion increases in speed with temperature, while the increase in *f* indicates that more molecules are reorienting on the OSIRIS timescale. The mean residency times of the protons are calculated as described in the ESI and presented in Table S6; again, these suggest the proton motion is faster in the Zn^{2+} compound than the Mn^{2+} analogue. With increasing temperature, the mean residency times reduce but without a discontinuity through the phase transition, consistent with the gradual increase in motion observed on the ^2H NMR timescale. Activation energies extracted from a plot of the evolution of $\ln \Gamma$ against inverse temperature yield estimated values for the activation energy for the motion observed as ~10 kJ·mol^{-1} for both compounds (see Figure S11). This activation energy is averaged across both ferroelectric and paraelectric phases due to the limited data available in the high temperature phase and thus primarily suggests that the preexponent of the Zn^{2+} phase is larger than for Mn^{2+}, given other aspects of the QENS analysis suggests motion is faster in the former.

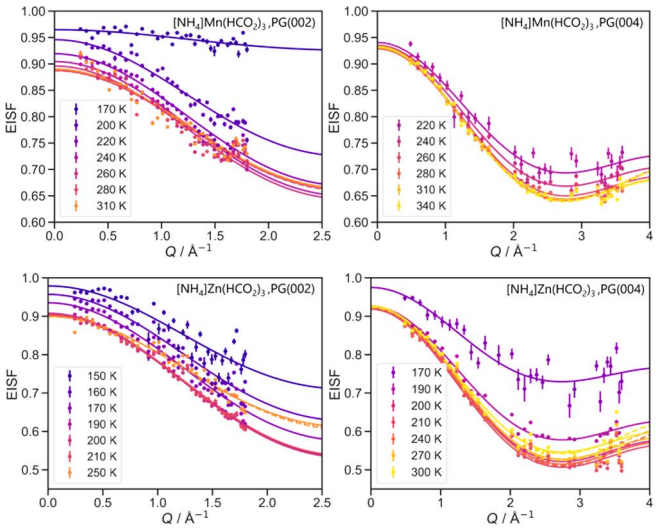

Figure 5 EISF plots for $[NH_4]M(HCO_2)_3$, where M = Mn^{2+} and Zn^{2+} in both the PG(002) and PG(004) analyser orientations, with models fitted to the experimental EISF data. Solid lines show model **E** (threefold rotation with a formate contribution), and dashed lines show model **F** (threefold rotation and twofold rotation) for higher temperatures. There are very small differences between the different models. See ESI for further details.

Origins of dielectric relaxation

The $NH_4M(HCO_2)_3$ series have channels of NH_4^+ cations which are likely screened from each other by the anionic framework. Similarly, within the channels the lack of hydrogen bonding between neighbouring NH_4^+ cations suggests they are relatively well isolated from each other, unlike in the related $[NH_3NH_2]Mg(HCO_2)_3$ where the larger molecular cations interact significantly.[23] Thus the hydrogen-bonding network formed with the anionic framework likely plays a key role in the NH_4^+ cations ordering at the phase transition. The greater motion of NH_4^+ cations in the Zn^{2+} material suggested by the QENS is likely responsible for its lower temperature phase transition compared to the Mn^{2+} compound because less thermal energy is required for the transition to the high temperature phase to occur. The channels of the Zn^{2+} phase are smaller than those in the Mn^{2+} phase (c.f. 8.3946(8) Å to 8.4461(11) Å based on the structures of Xu *et al.*[12]), as might be expected from the smaller ionic radii of Zn^{2+} (c.f. 0.74 Å and 0.83 Å for Zn^{2+} and Mn^{2+}, respectively).[26] It is thus unlikely that mechanical effects are primarily responsible for the greater motion of the Zn^{2+} phase; instead this likely involves subtle differences in the hydrogen bonding network between the NH_4^+ cations and the framework leading to these being stronger for the Zn phase, we are unable to resolve these differences within the precision of our crystal structures. The general trend of the structural phase transition decreasing in temperature with decreasing ionic size across the $[NH_4]M(HCO_2)_3$ series might be linked to the motion of the NH_4^+ cations increasing with smaller size B-site cations. In this case, the motion of these A-site cations in the Ni^{2+} framework may be sufficiently high to supress the phase transition completely.

Both the ^2H SSNMR and QENS data suggest that the motion is similar, albeit slower, in the low-temperature and high-temperature phases. To investigate this further, we used nudged elastic band calculations to estimate the energy barrier to reorientation

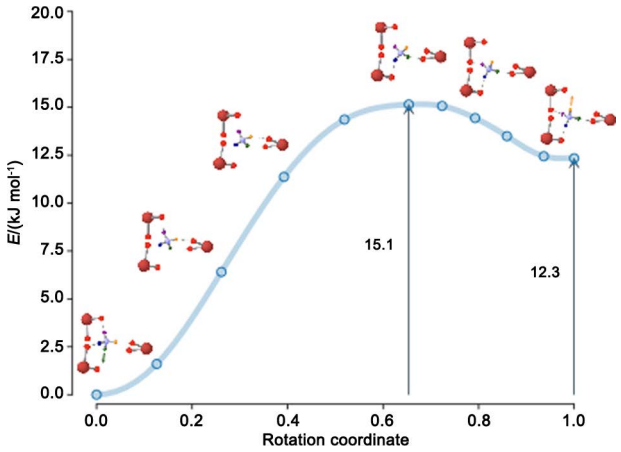

Figure 6 Change in energy, from DFT NEB calculations, as a single N1 NH_4^+ cation is rotated from its experimentally determined position (rotation coordinate 0.0) to an inverted orientation (rotation coordinate 1.0) in the low temperature phase of $[NH_4]Zn(HCO_2)_3$. As indicated in accompanying structure fragments, this involves a limited tilting of the tetrahedron rather than a C_2 rotation through a full 180°. The small arrows in initial and final structures indicate the direction of the *c*-axis, demonstrating that this motion indeed produces a transition between "up" and "down" states.

of a single N2 ammonium ion in the low-temperature phase of $[NH_4]Zn(HCO_2)_3$ under different motional models. It is clear from the NMR spectra that all the ammonium sites are undergoing essentially the same motion; while the diffraction data indicate that the N2 site is more disordered than others, it is clear the motion in the low temperature phase is not restricted to this site. As shown in Figure 6, we find a particularly low energy barrier of 15.2 $kJ{\cdot}mol^{-1}$ for a tilt-jump process that switches between "up" and "down" states while also converting between axial and equatorial sites, thus avoiding a full 180° rotation (see Video S1). Alternative mechanisms for inverting the ammonium orientation involve breaking more hydrogen bonds, *e.g.*, a C_3-like motion about the *c* axis, and have higher energy barriers (see Videos S2–3 & Figure S12). The energy barrier is similar in magnitude to the barrier to rotation in ammonium bromide, estimated at 14–18 $kJ{\cdot}mol^{-1}$;[40] interestingly, this is also approximately constant across the III-II order-disorder transition at 235 K in that material. A pair of "tilt-jumps" will return the cations to their original, low-energy, orientation, but crucially will scramble the N–H orientations. Hence, we propose that this low-energy process is responsible for the dynamics observed in the NMR and QENS experiments. In the low-temperature phase, the "flipped" state is 12.3 $kJ{\cdot}mol^{-1}$ above the ground-state structure and will have negligible equilibrium population (*i.e.*, will not be observed in experiments). Above the phase transition, there is no energy penalty for inverting an individual cation and the "up"/"down" states will be equally occupied, leading to the crystallographic disorder observed in the high temperature phase. Modelling the energetic profile in this phase, however, would require sophisticated molecular dynamics simulations and is outside the scope of this work. It is already clear from the NMR and QENS that the barrier to motion is lower in the high temperature phase. Such behaviour is commonly observed in both ionic and molecular "plastic crystals" and the negative thermal expansion material, ZrW_2O_8.[40-41] The fact that the same motional process allows dipole inversion and scrambling of the ammonium orientation in *both* phases provides an elegant rationalisation for the relaxor behaviour in the low-temperature polar phase, including both the shift with frequency and the broadness of the peak observed in the dielectric spectra. That the motion attributed to the "tilt-jump" is detectable on the slower timescale of the NMR, which are measured at 61.4 MHz, are particularly relevant as it broadly coincides with the timescale of the dielectric spectroscopy,[18] which are measured across a 1–1000 kHz range for both $[NH4]Mn(HCO_2)_3$ and $[NH_4]Zn(HCO_2)_3$.[12,14] This makes it likely this motion causes the previously reported dielectric relaxation. While a more detailed analysis of the effects of the proposed dynamics on the dielectric spectra would add further insight computational studies that predict the dielectric properties would be required to achieve this, this would be very computational expensive and thus beyond the scope of this study.

The lack of significant interactions between the NH_4^+ cations in the same channel likely plays a significant role in the relatively low barrier to reorientation, as there is no strong restriction preventing neighbouring molecular cations from adopting different orientations. Previous EPR work suggested this transition belongs to a 2D universality class;[27] this is probably associated with ordering of the crystallographically distinct channels within the *ab* plane while lone NH_4^+ cations within a channel may flip their orientations. The observed crystallographic disorder of the NH_4^+ molecules containing N2 in both phases potentially reflects a greater tendency to rotation. Ultimately our proposition is that there is a link between the disorder in the orientation of the NH_4^+ cations and their dielectric relaxation. That orientational disorder is responsible for that their relaxor-like dielectric relaxation is similar to $[NH_3NH_2]Mg(HCO_2)_3$, despite a number of differences between the reported origins of their ferroelectric polarisation and phase transitions.[23]

Conclusions

The structure of the ferroelectric phase of $[NH_4]M(HCO_2)_3$ frameworks has been clarified, with the three crystallographically distinct ammonium environments modelled by neutron diffraction. The hydrogen bond network is primarily between the NH_4^+ cations and the anionic framework, with very limited interactions between neighbouring molecular cations, suggesting that these are relatively well isolated from each other.

Both QENS and ^2H SSNMR studies show that the hydrogen sites of the ammonium ions rapidly "scramble". Motion gradually increases and becomes more isotropic with increasing temperature, strikingly with no clear change in the nature of the motion present at the crystallographic phase transition with a significant change in the rate of motion only visible on the faster QENS timescale. The activation energy of the ammonium motion extracted from relaxation studies decreases significantly in the paraelectric phase. QENS measurements show motion is local and broadly similar in the Mn^{2+} and Zn^{2+} phases, although faster in the latter, consistent with its lower ordering temperature. Nudged elastic band calculations suggest the barrier to "flipping" of the NH_4^+ molecules is relatively low in the low-temperature phase.

Combining these experimental and simulation results, we hypothesise that the "flipping" motion, possible in both the low- and high-temperature phases, may in fact be the primary motion responsible for scrambling the orientation of the NH_4^+ cations in the channels, thereby causing the significant dielectric relaxation consistent with relaxor-like ferroelectricity. Our results suggest that *rotational* disorder may be an effective substitution for *compositional* disorder in designing new relaxor ferroelectric framework materials. While further studies of other framework materials known to exhibit significant dielectric relaxation are required to confirm if such rotational disorder is common to these, if this is the case it highlights a new route to relaxor ferroelectrics that is inherently linked to these being molecular materials. Establishing this as a design criteria and how different extents and forms of rotational disorder affect the extent of dielectric relaxation should pave the way towards next-generation relaxor ferroelectrics.

Experimental

Samples of $[NH_4]M(HCO_2)_3$, where M = Mn^{2+} and Zn^{2+}, were

produced by slow diffusion reactions following literature methods.[12,14,42-43] Mn^{2+} samples were produced by layering $Mn(ClO_4)_2{\cdot}4H_2O$, 0.1 M, over a combination of formic acid, 0.4 M, and NH_4CO_2H, 0.8 M in methanol, 16 mL. Powder samples for QENS were produced by combining multiple batches.[43] Zn^{2+} samples were produced by the same layering method with $Zn(ClO_4)_2{\cdot}4H_2O$, 0.2 M, over a combination of formic acid, 0.8 M, and NH_4CO_2H, 2.4 M in dried methanol, 16 mL. QENS samples were produced by a scaled-up synthesis in 40 mL of dried methanol. These samples are all undeuterated. Colourless single crystals were produced for SCND of ~1 mm^3 for M = Mn^{2+} and ~4 mm^3 for M = Zn^{2+}. Powder diffraction patterns were collected on a Rigaku Miniflex benchtop diffractometer, with Le Bail refinements confirming the purity of the samples found in the ESI as Figures S13 and S14. Single-crystal neutron diffraction measurements were done using the SXD diffractometer and QENS measurements using the OSIRIS spectrometer, both at the ISIS neutron source (see ESI for further experimental details).[44-45]

^2H NMR spectra were obtained on a Bruker Avance III HD spectrometer operating at a ^2H NMR frequency of 61.42 MHz. Samples were packed into 4 mm zirconia rotors. The ^2H shift scale was referenced with respect to neat TMS by setting the peak of a replacement sample of D_2O to 4.81 ppm. Variable-temperature ^2H wideline (static) spectra were acquired using a solid echo with a 10 s recycle delay and 40 µs echo delay, starting at ambient temperature and cooling in stages down to −109 °C (calibrated temperature). Reproducibility of the spectra was observed on warming the sample to ambient temperature. The lineshapes corresponded to symmetric quadrupole coupling tensors (*i.e.*, negligible asymmetry factor/rhombicity, η), and so the effective ^2H quadrupolar coupling, C_Q, could be simply obtained from the separation of the peaks, $\Delta\nu$, using $C_Q = 4\Delta\nu/3$. Note that this analysis assumes a single dominant value of C_Q.

T_1 relaxation times were measured using a saturation recovery sequence (saturation with 64 90° pulses separated by 1 ms), again using a 40 µs solid echo for detection. Relaxation time constants were obtained by fitting spectral integrals to a general exponential recovery function. Conversion between set temperatures and actual sample temperatures was done by independent calibration experiments using ethylene glycol. Uncertainties in the final absolute sample temperatures are estimated to be ±5 K. Further details of the analysis and temperature calibration can be found in the data archive at https://data.kent.ac.uk/id/eprint/549.

Density-functional theory calculations were performed for $[NH_4]Zn(HCO_2)_3$ using CASTEP academic release v. 24.1,[46] using the PBE functional[47] with TS semi-empirical dispersion correction.[48-49] This software uses the plane-wave pseudopotential method: ultrasoft pseudopotentials were generated on the fly using default settings, while the plane-wave basis set cutoff was set to 751 eV; the fine grid used to represent the core and augmentation charge density was set to three times the diameter of the cutoff sphere. Each energy calculation was converged to within 10^{-8} eV/atom, and the geometry optimisations were converged to a maximum energy change of 2×10^{-5} eV/atom, a maximum force of 0.05 eV/Å, and a maximum shift of 0.001 Å. A single unit cell was modelled using periodic boundary conditions, with cell parameters fixed at their experimental geometry. First, all atomic positions allowed to refine within the experimental $P6_3$ symmetry. Next, a geometry in which one N1 ammonium ion was flipped was generated, and again all atomic positions were allowed to refine within the resulting $P3$ symmetry. Finally, a nudged elastic band calculation between these local minima was performed in $P1$ symmetry. The H atoms were identified between the two end states to minimise the distance travelled; in particular, this means that the flip takes the apical site to an equatorial site and *vice versa* (Video S1). Nine intermediate states were refined, with the central one constrained to move uphill to the transition state.

Supporting Information

The supporting information for this article is available on the WWW under https://doi.org/10.1002/cjoc.202401192.

Acknowledgement

EPSRC funded this project through a PhD studentship for TJH. PH and HMW were supported during this work through a Project Grant from the Leverhulme Trust (RPG-2018-288). Neutron diffraction and QENS experiments at the ISIS Pulsed Neutron and Muon Source were supported by a beamtime allocation from the Science and Technology Facilities Council (RB 1820062 and 1910402). We are grateful to the UK Materials and Molecular Modelling Hub for computational resources, which is partially funded by EPSRC (EP/T022213/1, EP/W032260/1 and EP/P020194/1).

References

[1] Cohen, R. E. Origin of ferroelectricity in perovskite oxides. *Nature* **1992**, *358*, 136–138.
[2] Haertling, G. H. Ferroelectric Ceramics: History and Technology. *J. Am. Ceram. Soc.* **1999**, *82*, 797–818.
[3] Horiuchi, S.; Kumai, R.; Tokura, Y. Proton-displacive ferroelectricity in neutral cocrystals of anilic acids with phenazine. *J. Mater. Chem.* **2009**, *19*, 4421–4434.
[4] Horiuchi, S.; Kumai, R.; Tokura, Y. Hydrogen-bonded donor–acceptor compounds for organic ferroelectric materials. *Chem. Commun.* **2007**, 2321–2329.
[5] Pramanick, A.; Osti, N. C.; Jalarvo, N.; Misture, S. T.; Diallo, S. O.; Mamontov, E.; Luo, Y.; Keum, J. K.; Littrell, K. Origin of dielectric relaxor behavior in PVDF-based copolymer and terpolymer films. *AIP Adv.* **2018**, *8*, 045204.
[6] Cowley, R. A.; Gvasaliya, S. N.; Lushnikov, S. G.; Roessli, B.; Rotaru, G. M. Relaxing with relaxors: a review of relaxor ferroelectrics. *Adv. Phys.***2011**, *60*, 229–327.
[7] Wook, J.; Dittmer, R.; Acosta, M.; Zang, J.; Groh, C.; Sapper, E.; Wang, K.; Rödel, J. Giant electric-field-induced strains in lead-free ceramics for actuator applications-status and perspective. *J. Electroceram.* **2012**, *29*, 71–93.
[8] Gadinski, M. R.; Li, Q.; Zhang, G.; Zhang, X.; Wang, Q. Understanding of relaxor ferroelectric behavior of poly(vinylidene fluoride-trifluoroethylene-chlorotrifluoroethylene) terpolymers. *Macromolecules* **2015**, *48*, 2731–2739.
[9] Ahn, C. W.; Hong, C.-H.; Choi, B.-Y.; Kim, H.-P.; Han, H.-S.; Hwang, Y.; Jo, W.; Wang, K.; Li, J.-F.; Lee, J.-S.; Kim, I. W. A brief review on relaxor ferroelectrics and selected issues in lead-free relaxors. *J. Korean Phys. Soc.* **2016**, *68*, 1481–1494.
[10] Egami, T. Local Structure of Ferroelectric Materials. *Ann. Rev. Mater. Res.* **2007**, *37*, 297–315.
[11] Cross, L. E. Relaxor ferroelectrics: an overview. *Ferroelectrics* **1994**, *151*, 305–320.
[12] Xu, G.-C.; Zhang, W.; Ma, X.-M.; Chen, Y.-H.; Zhang, L.; Cai, H.-L.; Wang, Z.-M.; Xiong, R.-G.; Gao, S. Coexistence of Magnetic and Electric Orderings in the Metal–Formate Frameworks of $[NH_4][M(HCOO)_3]$. *J. Am. Chem. Soc.* **2011**, *133*, 14948–14951.
[13] Fu, D.-W.; Zhang, W.; Cai, H.-L.; Zhang, Y.; Ge, J.-Z.; Xiong, R.-G.; Huang, S. D.; Nakamura, T.; Fu, D.; Zhang, W.; Cai, H.; Zhang, Y.; Ge, J.; Xiong, R.; Huang, S. D.; Nakamura, T. A Multiferroic Perdeutero Metal–Organic Framework. *Angew. Chem. Int. Ed.* **2011**, *50*, 11947–11951.
[14] Xu, G. C.; Ma, X. M.; Zhang, L.; Wang, Z. M.; Gao, S. Disorder-order ferroelectric transition in the metal formate framework of $[NH_4][Zn(HCOO)_3]$. *J. Am. Chem. Soc.* **2010**, *132*, 9588–9590.
[15] Chen, S.; Shang, R.; Hu, K.-L.; Wang, Z.-M.; Gao, S. $[NH_2NH_3][M(HCOO)_3]$ (M = Mn^{2+}, Zn^{2+}, Co^{2+} and Mg^{2+}): structural

phase transitions, prominent dielectric anomalies and negative thermal expansion; magnetic ordering. *Inorg. Chem. Front.* **2014**, *1*, 83–98.

[16] Shi, C.; Ma, J. J.; Jiang, J. Y.; Hua, M. M.; Xu, Q.; Yu, H.; Zhang, Y.; Ye, H. Y. Large Piezoelectric Response in Hybrid Rare-Earth Double Perovskite Relaxor Ferroelectrics. *J. Am. Chem. Soc.* **2020**, *142*, 9634–9641.

[17] Shang, R.; Chen, S.; Hu, K.-L.; Wang, B.-W.; Wang, Z.-M.; Gao, S. A Variety of Phase-Transition Behaviors in a Niccolite Series of $[NH_3(CH_2)_4NH_3][M(HCOO)_3]_2$. *Chem. Eur. J.* **2016**, *22*, 6199–6203.

[18] Berlie, A.; Terry, I.; Szablewski, M.; Telling, M.; Apperley, D.; Hodgkinson, P.; Zeller, D. A study of the dynamics and structure of the dielectric anomaly within the molecular solid $TEA(TCNQ)_2$. *Phys. Chem. Chem. Phys.* **2022**, *24*, 7481–7492.

[19] Xu, W.-J.; Kopyl, S.; Kholkin, A.; Rocha, J. Hybrid organic-inorganic perovskites: Polar properties and applications. *Coord. Chem. Rev.* **2019**, *387,* 398–414.

[20] Shi, C.; Han, X.-B.; Zhang, W. Structural phase transition-associated dielectric transition and ferroelectricity in coordination compounds. *Coord. Chem. Rev.* **2019**, *378*, 561–576.

[21] Bovill, S. M.; Saines, P. J. Structure and magnetic properties of the $AB(HCO_2)_3$ (A = Rb^+ or Cs^+, B = Mn^{2+}, Co^{2+} or Ni^{2+}) frameworks: probing the effect of size on the phase evolution of the ternary formates. *CrystEngComm* **2015**, *17*, 8319–8326.

[22] Boström, H. L. B.; Senn, M. S.; Goodwin, A. L. Recipes for improper ferroelectricity in molecular perovskites. *Nat. Commun.* **2018**, *9*, 1–7.

[23] Hitchings, T. J.; Wickins, H. M.; Peat, G. U. L.; Hodgkinson, P.; Srivastava, A. K.; Lu, T.; Liu, Y.; Piltz, R. O.; Demmel, F.; Phillips, A. E.; Saines, P. J. A new avenue to relaxor-like ferroelectric behaviour found by probing the structure and dynamics of $[NH_3NH_2]Mg(HCO_2)_3$. *J. Mater. Chem. C* **2023**, *11*, 9695–9706.

[24] Maïczka, M.; Pietraszko, A.; Macalik, B.; Hermanowicz, K. Structure, phonon properties; order-disorder transition in the metal formate framework of $[NH_4][Mg(HCOO)_3]$. *Inorg. Chem* .**2014**, *53*, 787–794.

[25] Lawler, J. M. M.; Manuel, P.; Thompson, A. L.; Saines, P. J. Probing ferroic transitions in a multiferroic framework family: a neutron diffraction study of the ammonium transition metal formates. *Dalton Trans.* **2015**, *44*, 11613–11620.

[26] Shannon, R. D. Revised Effective Ionic Radii and Systematic Studies of Interatomie Distances in Halides and Chaleogenides. *Acta Cryst.* **1976**, *32*, 751–767.

[27] Navickas, M.; Giriūnas, L.; Kalendra, V.; Biktagirov, T.; Gerstmann, U.; Schmidt, W. G.; Mączka, M.; Pöppl, A.; Banys, J.; Šimėnas, M. Electron paramagnetic resonance study of ferroelectric phase transition and dynamic effects in a Mn^{2+} doped $[NH_4][Zn(HCOO)_3]$ hybrid formate framework. *Phys. Chem. Chem. Phys.* **2020**, *22*, 8513–8521.

[28] Xu, J.; Lucier, B. E. G.; Sinelnikov, R.; Terskikh, V. V.; Staroverov, V. N.; Huang, Y. Monitoring and Understanding the Paraelectric–Ferroelectric Phase Transition in the Metal–Organic Framework $[NH_4][M(HCOO)_3]$ by Solid-State NMR Spectroscopy. *Chem. Eur. J.* **2015**, *21*, 14348–14361.

[29] Vit, V.; Scaravonati, S.; Cugini, F.; Pontiroli, D.; Orlandi, F.; Solzi, M.; Riccò, M.; Righi, L. Proton-conduction under mild humid conditions in $[NH_4][M(HCOO)_3]$ (M=Mn^{2+}, Co^{2+}) frameworks. *J. Solid State Chem.* **2024**, *338*, 124911.

[30] Duncan, H. D.; Dove, M. T.; Keen, D. A.; Phillips, A. E. Local structure of the metal–organic perovskite dimethylammonium manganese(II) formate. *Dalton Trans.* **2016**, *45*, 4380–4391.

[31] Chen, S.; Shang, R.; Hu, K.-L.; Wang, Z.-M.; Gao, S. $[NH_2NH_3][M(HCOO)_3]$ (M = Mn^{2+}, Zn^{2+}, Co^{2+} and Mg^{2+}): structural phase transitions, prominent dielectric anomalies and negative thermal expansion; magnetic ordering. *Inorg. Chem. Front.* **2014**, *1*, 83–98.

[32] Yildirim, A.; Krause, C.; Zorn, R.; Lohstroh, W.; Schneider, G. J.; Zamponi, M.; Holderer, O.; Frick, B.; Schönhals, A. Complex molecular dynamics of a symmetric model discotic liquid crystal revealed by broadband dielectric, thermal and neutron spectroscopy. *Soft Matter* **2020**, *16*, 2005–2016.

[33] Khaneft, M.; Holderer, O.; Ivanova, O.; Lüke, W.; Kentzinger, E.; Appavou, M. S.; Zorn, R.; Lehnert, W. Structure and Proton Dynamics in Catalytic Layer of HT-PEFC. *Fuel Cells* **2016**, *16*, 406–413.

[34] Willis, B. T. M.; Pryor, A. W. *Thermal Vibrations in Crystallography*, Cambridge University Press: Cambridge, **1975**.

[35] Bée, M. *Quasielastic neutron scattering*: *Principles and applications in solid state chemistry, biology and materials science*, Adam Hilger, IOP Publishing: Bristol and Philadelphia, **1989**.

[36] Leguy, A. M. A.; Frost, J. M.; McMahon, A. P.; Sakai, V. G.; Kockelmann, W.; Law, C.; Li, X.; Foglia, F.; Walsh, A.; O'Regan, B. C.; Nelson, J.; Cabral, J. T.; Barnes, P. R. F. The dynamics of methylammonium ions in hybrid organic–inorganic perovskite solar cells. *Nat. Commun.* **2015**, *6*, 7124.

[37] Lavén, R.; Häussermann, U.; Perrichon, A.; Andersson, M. S.; Targama, M. S.; Demmel, F.; Karlsson, M. Diffusional Dynamics of Hydride Ions in the Layered Oxyhydride $SrVO_2H$. *Chem. Mater.* **2021**, *33*, 2967–2975.

[38] Meijer, B. E.; Cai, G.; Demmel, F.; Walker, H. C.; Phillips, A. E. Pressure dependence of rotational dynamics in barocaloric ammonium sulfate. *Phys. Rev. B* **2022**, *106*, 064302.

[39] Verdal, N.; Hartman, M. R.; Jenkins, T.; Devries, D. J.; Rush, J. J.; Udovic, T. J. Reorientational dynamics of $NaBH_4$ and KBH_4. *J. Phy. Chem. C* **2010**, *114*, 10027–10033.

[40] Parsonage, N. G.; Staveley, L. A. K. *Disorder in Crystals*, Clarendon Press: Oxford, **1978**.

[41] Hampson, M. R.; Evans, J. S. O.; Hodgkinson, P. Characterization of Oxygen Dynamics in ZrW_2O_8. *J. Am. Chem. Soc.* **2005**, *127*, 15175–15181.

[42] Collings, I. E.; Bykov, M.; Bykova, E.; Tucker, M. G.; Petitgirard, S.; Hanfland, M.; Glazyrin, K.; Smaalen, S.; van, Goodwin, A. L.; Dubrovinsky, L.; Dubrovinskaia, N. Structural distortions in the high-pressure polar phases of ammonium metal formates. *CrystEngComm* **2016**, *18*, 8849–8857.

[43] Burley, L. G. *Exploring the Structures and Dynamics of Amine-Templated Formate Frameworks*, University of Kent, **2019**.

[44] Telling, M. T. F.; Andersen, K. H. Spectroscopic characteristics of the OSIRIS near-backscattering crystal analyser spectrometer on the ISIS pulsed neutron source. *Phys. Chem. Chem. Phys.* **2005**, *7*, 1255–1261.

[45] Keen, D. A.; Gutmann, M. J.; Wilson, C. C. SXD – the single-crystal diffractometer at the ISIS spallation neutron source. *J. Appl. Crystallogr.* **2006**, *39*, 714–722.

[46] Clark, S. J.; Segall, M. D.; Pickard, C. J.; Hasnip, P. J.; Probert, M. I. J.; Refson, K.; Payne, M. C. First principles methods using CASTEP. *Z. Kristallogr.* **2005**, *220*, 567–570.

[47] Perdew, J. P.; Burke, K.; Ernzerhof, M. Generalized Gradient Approximation Made Simple. *Phys. Rev. Lett.* **1996**, *77*, 3865–3868.

[48] Tkatchenko, A.; Scheffler, M. Accurate Molecular Van Der Waals Interactions from Ground-State Electron Density and Free-Atom Reference Data. *Phys. Rev. Lett.* **2009**, *102*, 73005.

[49] McNellis, E. R.; Meyer, J.; Reuter, K. Azobenzene at coinage metal surfaces: Role of dispersive van der Waals interactions. *Phys. Rev. B* **2009**, *80*, 205414.

Manuscript received: November 22, 2024
Manuscript revised: January 30, 2025
Manuscript accepted: February 5, 2025
Version of record online: XXXX, 2025

The Authors

Left to Right: (Top) Thomas J. Hitchings, Helen M. Wickins, Lydia G. Burley, Silvia C. Capelli, (Bottom) Franz Demmel, Anthony E. Phillips, Paul Hodgkinson and Paul J. Saines

